Effects of polymer matrices to the formation of silicon carbide (SiC) nanoporous fibers and nanowires under carbothermal reduction

Ping Lu[†], Qing Huang[‡§], Amiya Mukherjee[‡] and You-Lo Hsieh*[†]

[†] Fiber and Polymer Science, University of California, Davis, California 95616, USA

[‡] Department of Chemical Engineering & Materials Science, University of California, Davis, California 95616, USA

[§] Ningbo Institute of Material Technology & Engineering, Chinese Academy of Sciences, Ningbo, China

* To whom correspondence should be addressed. Tel.: +1 530 752 0843. E-mail: ylhsieh@ucdavis.edu.

Graphical contents

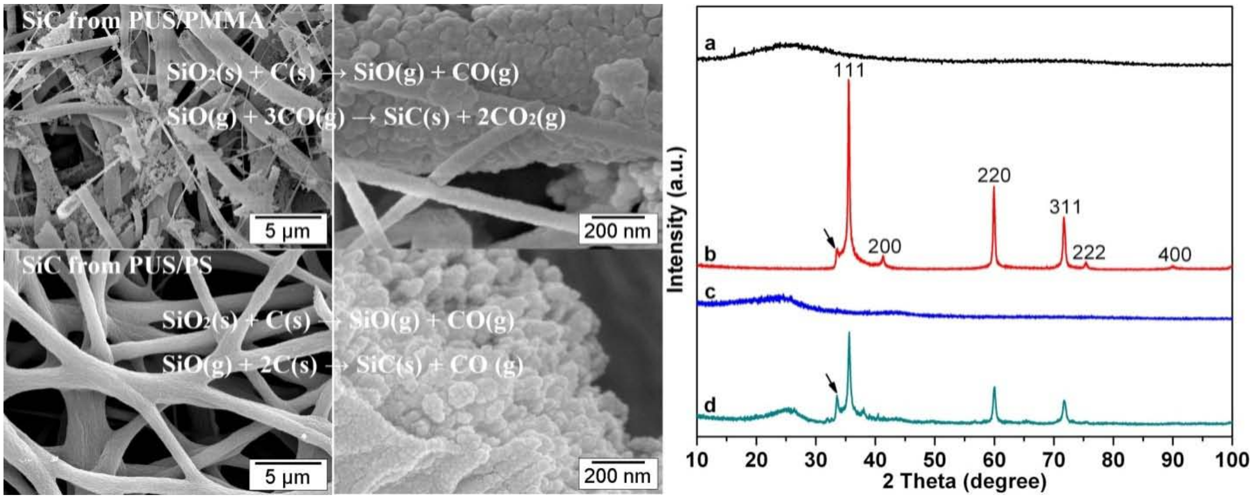

Nanoporous silicon carbide (SiC) fibers and nanowires from carbothermal reduction of polyureasilazane (PUS) hybrids

Abstract

SiC fibers with varied nano-scale morphologies (i.e., nanowires, nanoparticles, etc) were successfully fabricated by electrospinning of preceramic polyureasilazane (PUS) with either poly(methyl methacrylate) (PMMA) or polystyrene (PS) into composite fibers that were subsequently carbothermally reduced to ceramics via pyrolysis in argon at 1560ºC. While SiC fibers from either composite fibers contained polycrystalline cubic SiC (β-SiC) structure, their fiber morphologies and atomic compositions differed due to the distinct thermal behaviors and decomposition pathways of PMMA and PS. Pyrolysis at 1000ºC produced fibrous mats of amorphous SiCO from PUS/PMMA with high O (32.5%) content or from PUS/PS with high C (74.7%) content. These differences led to distinct SiC fiber morphologies from further pyrolysis at 1560ºC, i.e., an interconnected fibrous mat of nanoparticle-filled porous core and wrinkled sheath fibers from PUS/PS and fragmented nanoparticle-filled porous fibers intermixed with abundant 100 nm diameter nanowires with straight, beaded and bamboo-like morphologies from PUS/PMMA.

Keywords: Nanoporous SiC sheath-core fibers, SiC nanowires, carbothermal reduction, β-SiC

Introduction

Silicon carbide (SiC), one of the most important semiconductor materials formed by covalent bonding between Si and C, has been the material of choice for high-power, high-frequency, and high-temperature applications in harsh environments due to its wide band gap (~3.2 eV), large breakdown electric field strength (>2 MV cm^{-1}, 10 times that of silicon), high electron mobility (~900 cm^{2} V^{-1} s^{-1}), high electron saturation velocity (2-2.5×10^{7} cm/s, twice that of silicon), and high thermal conductivity (5-7 W cm^{-1} K^{-1}, close to that of metals such as Ag or Cu).[1-4] These advantages, along with high mechanical strength, excellent resistance to oxidation and chemical stability at elevated temperatures, also make SiC a promising material as heterogeneous catalyst supports.[5-7] However, the low surface area of SiC (around 1 m^{2}/g) synthesized by conventional high temperature process is the main hindrance to this area of application.[8, 9]

Porous SiC has, thus, become a focus of recent research as catalyst supports as well as for diversifying its applications in extreme conditions, such as filters for molten metal, hot gas or diesel particulate, thermal insulators, gas-burner media, and light-weight structural materials, utilizing its low thermal expansion coefficient, high thermal shock resistance, and excellent abrasion resistance.[9-13] A number of processes, generally categorized into replica, sacrificial template and reaction techniques, have been developed to prepare porous SiC ceramics with tuned porosity, pore size, and degree of interconnectivity to satisfy the associated requirements for specific applications.[14-22] Nanoporous SiC prepared by replica technique using mesoporous silica as the template had 780 m^2/g specific surface.[23] Pyrolysis of polycarbosilane infiltrated in egg shell, butterfly wing, and sea urchin skeleton has shown to generate porous structures unique to these biological templates.[24] Monolithic SiC with macropores from 0.1-1.5 μm were successfully obtained from intramolecular carbothermal reduction of porous phenyl-bridged polysilsesquioxane via sol-gel preparation.[25] Porous SiC fibers have been prepared by electrospinning of preceramic polymers with fiber-forming template polymers, followed by pyrolytic conversion to inorganic ceramics.[26-30] Single-crystalline SiC nanofibers with thin SiO_2 surface layer were fabricated by carbothermal reduction of electrospun poly(vinyl pyrrolidone)/tetraethyloxysilane (PVP/TEOS) composite fibers.[30]

We previously prepared nanoporous SiCO fibers with sheath-core structures from electrospinning the preceramic polyureasilazane (PUS) precursor with poly(methyl methacrylate) (PMMA) followed by pyrolysis of the PUS/PMMA composite fibers at 500ºC.[31] The luffa-like surfaces of these silicon-containing fibers led to superhydrophobicity and their nanoporosity produced super-absorbency to hydrocarbon liquids. This study was initially aimed to fabricate SiC fibers by pyrolyzing the PUS/PMMA composite fibers at higher temperatures. However, the unexpected collapse of the three-dimensional fibrous structure from heating at 1560ºC raised the question on the thermal property of PMMA and led to the inclusion of the higher melting polystyrene (PS) for comparison. Therefore, the structural transformation and conversion of the electrospun PUS/PMMA and PUS/PS composite fibers to SiC by pyrolysis at 1000 and 1560ºC in inert atmosphere were studied. In this paper, the effects of carbon content to the structural stability of the sheath-core fibers in the conversion of SiCO to SiC as well as the formation of SiC nanowires were investigated and the possible mechanism was proposed.

Experimental

Chemical and materials

Poly(methyl methacrylate) (PMMA) (M_w = 120 k*Da*) and polystyrene (PS) (M_w = 350 k*Da*) were purchased from Sigma-Aldrich Chemical Company Inc. (Milwaukee, WI). Polyureasilazane (PUS) (KDT Ceraset, KiON Defense Technologies, Inc.) was the preceramic precursor to prepare silicon carbide (SiC). Acetone, N, N-dimethylformamide (DMF) and ethanol, from EMD Chemicals, were used as received without further purification. All water used was purified by Milli-Q plus water purification system (Millipore Corporate, Billerica, MA).

Electrospinning of PUS composite fibers

Mixtures of preceramic PUS with either PMMA (5/15 w/w PUS/PMMA in acetone) or PS (5/20 w/w PUS/PS in DMF) were prepared at 20 wt % or 25 wt% total polymer concentration, respectively, by vigorously stirring for 24 h. The 5/15 PUS/PMMA mixture was loaded into a 20 mL syringe (National Scientific) fitted with a 23 gauge inner diameter flat metal needle (BD Medical Franklin Lakes, NJ) and delivered at 10 mL/h with a syringe pump (KDS 200, KD Scientific, USA) while the 5/20 PUS/PS mixture was fed at 1 mL/h. Each mixture was electrospun by applying a constant voltage (18 kV for PUS/PMMA and 15 kV for PUS/PS) using a DC power supply (ES 30-0.1 P, Gamma High Voltage Research Inc., Ormond Beach, FL) to a horizontally positioned metal needle. The charged jet sprayed into fine fibers that were collected on a vertical aluminum plate (30 cm × 30 cm) placed 25 cm from the tip of the needle at 23.9ºC and 34% relative humidity. The electrospun fibrous membrane was dried at ambient temperature under vacuum for 24 h for the subsequent experiments.

Pyrolysis of PUS composite fibers

The electrospun PUS/PMMA and PUS/PS composite fibers were pyrolyzed in argon using a tube furnace (Mini-Mite, Lindberg/Blue). The samples were first heated at 10ºC/min to 120ºC, incubated for 60 min to stabilize the fiber structures, then heated at 5ºC/min to either 1000ºC or 1560ºC and held for 3 h.

Characterization

The microstructures and surface morphologies of the as-spun and pyrolyzed products were examined by a scanning electron microscope (SEM) (XL 30-SFEG, FEI/Philips, USA) after 2-min gold coating (Bio-Rad SEM coating system). For observation under a transmission electron microscope (TEM, Philips CM-12), the PUS/PMMA composite fibers pyrolyzed at 1560ºC were sonicated in ethanol for 20 min to separate the SiC nanowires from the broken nanoporous sheath-core fibers and disperse in solution. Several drops of the upper suspension were immediately placed on the carbon coated TEM grid and dried. The diameters of the SiC sheath-core fibers and nanowires were taken from 100 fibers by an image analyzer (analySIS FIVE, Soft Imaging System). The element distribution and atomic ratios of carbon, oxygen, and silicon in the pyrolyzed fibers were mapped and calculated by the energy-dispersive X-ray spectrometer (EDS) adjunct to the SEM at 25 kV emission voltage with a 5-mm working distance (X-ray focus plane). The crystalline phases were determined by X-ray diffraction (XRD) (Scintag XDS 2000 powder diffractometer) of the powder samples at 45 kV and 40 mA from 10° to 100° with a Ni-filtered Cu $K\alpha_1$ radiation (λ = 1.542 Å) and the selected area electron diffraction (SAED) pattern of SiC nanowires were captured using TEM diffraction mode operated at 120 kV. The Fourier transform infrared (FTIR) spectra were collected from 128 scans at a 4 cm^{-1} resolution from 4000 to 400 cm^{-1} using a Nicolet 6700 spectrometer (Thermo Fisher Scientific, USA). Raman spectra were recorded from 200 to 2000 cm^{-1} using an argon laser at 514 nm in 2D model by a Renishaw RM1000 spectrophotometer coupled with a Leica CCD detector. The thermal decomposition behaviors of PMMA and PS, and conversions of PUS/PMMA and PUS/PS to ceramics were recorded in N_2 at 10°C/min from 30 to 600°C by differential scanning calorimetry (DSC) (DSC-60, Shimadzu, Japan) and from 30 to 1000°C by thermogravimetric analysis (TGA-50, Shimadzu, Japan).

Results and discussion

Morphological transformation from pyrolysis

The as-spun PUS/PMMA and PUS/PS composite fibers were straight and became thinner and more irregular when pyrolyzed, especially at the higher temperature (Fig. 1). The as-spun PUS/PMMA fibers were slightly larger and more varied in sizes than the as-spun PUS/PS fibers (Fig. 2). Pyrolysis at 1000ºC reduced fiber sizes significantly in both cases and the lowering in the mean fiber diameter was more pronounced for PUS/PS, i.e., from 2.37 to 1.03 μm or a 56.5% reduction, as compared to the 41.5% reduction (2.75 to 1.61 μm) for PUS/PMMA. Pyrolysis at 1560ºC did not cause further size reduction for PUS/PS but reduced the diameters of PUS/PMMA fibers further to 1.13 μm or by another 29.8%. The fibrous mat of PUS/PMMA pyrolyzed at 1560ºC also fragmented substantially (Fig. 3a), while that of PUS/PS retained its fibrous structure and fiber size essentially (Fig. 1f). In fact, PUS/PS fibers pyrolyzed at 1000ºC were fused into interconnected network that remains similar at 1560ºC.

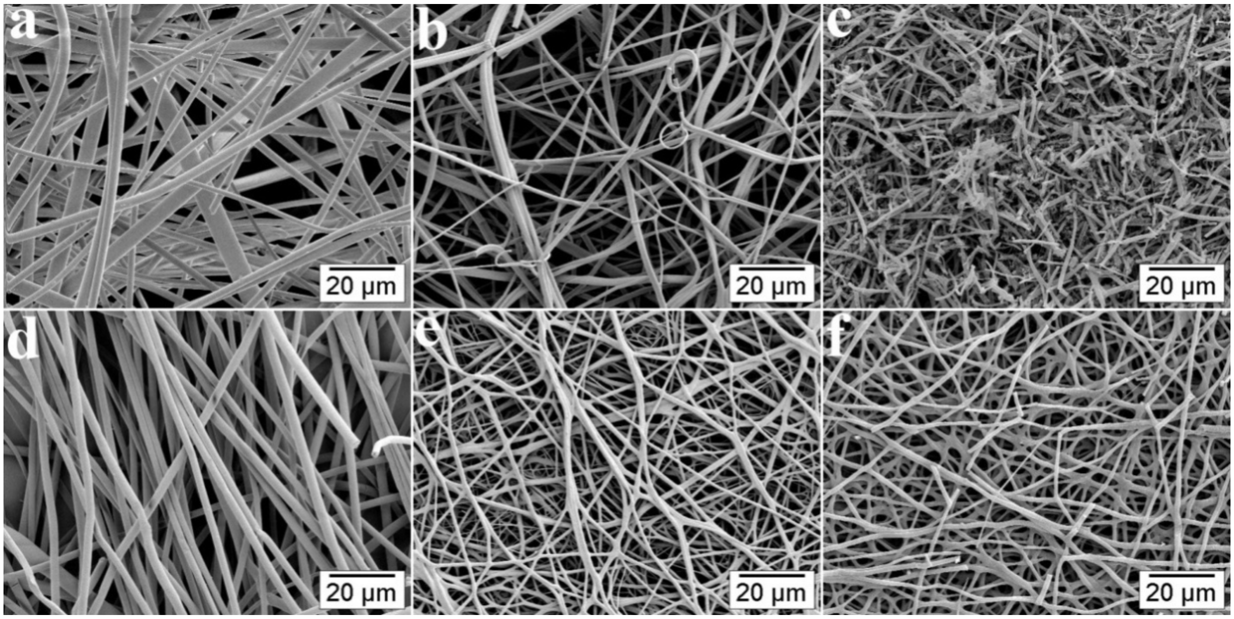

Fig. 1 SEMs of as-spun (a,d) and pyrolyzed (b,c,e,f) fibers: (a) as-spun 5/15 PUS/PMMA, pyrolyzed at (b) 1000ºC and (c) 1560ºC; (d) as-spun 5/20 PUS/PS, pyrolyzed at (e) 1000ºC and (f) 1560ºC. Pyrolysis was conducted in argon for 3 h.

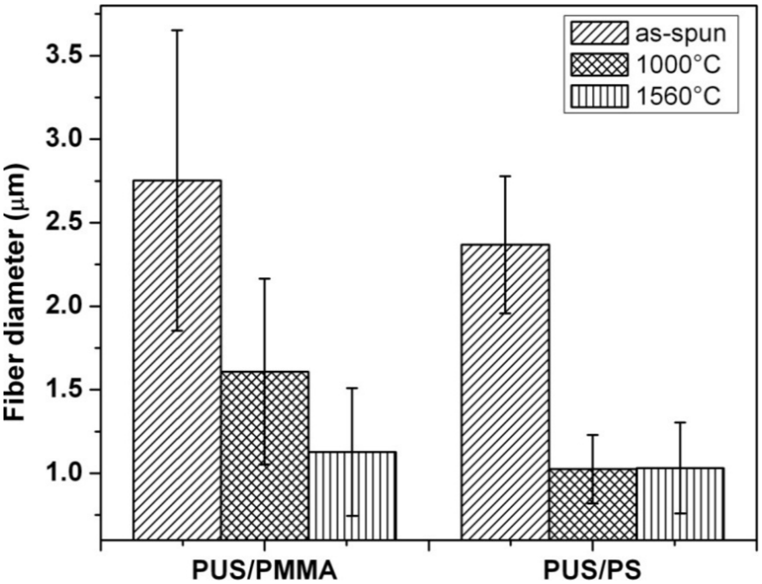

Fig. 2 Fiber diameters of as-spun composite and corresponding pyrolyzed fibers.

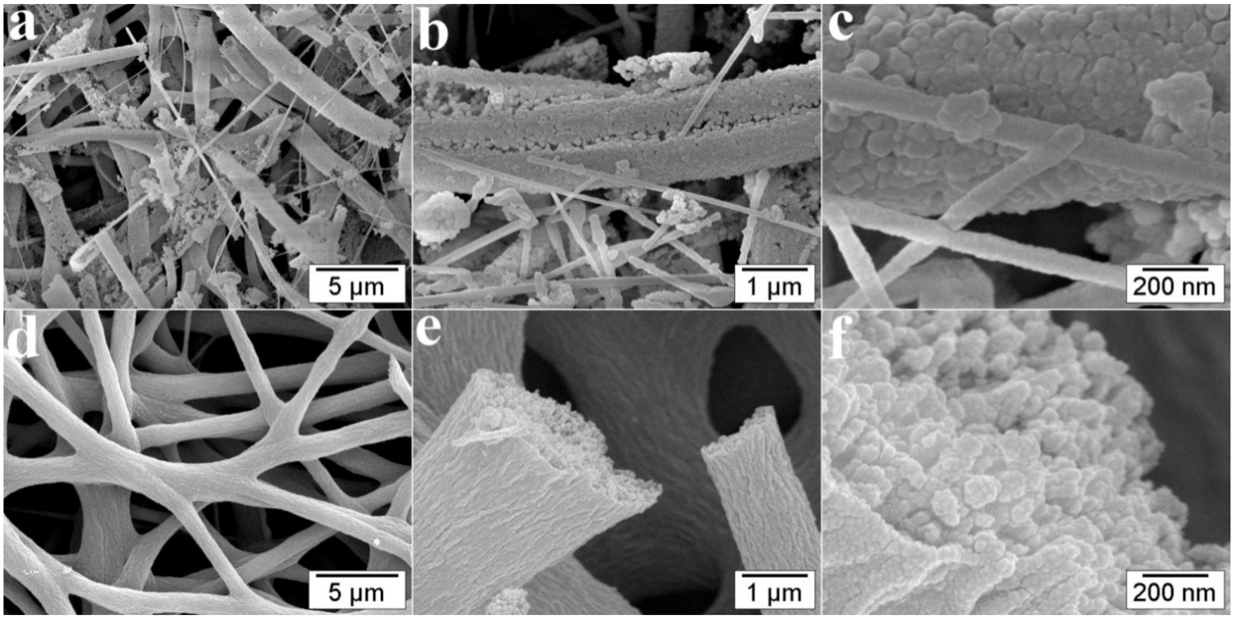

Fig. 3 SEMs of pyrolyzed (1560ºC for 3 h in argon) fibers from: (a, b, c) 5/15 PUS/PMMA, showing the collapsed fibrous structure and nanowires; (d, e, f) 5/20 PUS/PS, showing interconnected 3D fibrous mat and sheath-core fiber structures.

Closer examination of the composite fibers pyrolyzed at 1560ºC showed more specific structural differences. The pyrolyzed PUS/PMMA exhibited substantial fragments of nanoparticle-filled fiber segments, nanoparticle clusters and nanorods (Fig. 3a-c). Some fibers were split apart along the fiber axes, showing densely packed nanoparticles and porous centers (Fig. 3b,c). The pyrolyzed PUS/PS was a 3D interconnected fibrous mat with fibers showing patterned wrinkled shells and nanoparticle-filled core (Fig. 3d-f). This sheath-core fiber morphology from pyrolyzing PUS/PS at either 1000 or 1560ºC is similar to the luffa-like morphology of SiCO fibers we reported from calcination of PUS/PMMA at 500°C.[31]

Nanowire morphology

The most interesting distinction between the two composite fibers was the abundant nanowires with length up to several hundred micrometers (Fig. 3a-c, 4a) from pyrolysis of PUS/PMMA at 1560ºC. Nanowire was absent from pyrolyzed PUS/PS (Fig. 3f). Further observation of these nanowires by SEM (Fig. 4) and TEM (Fig. 5) showed three distinctive shapes: straight, beaded, and bamboo-like, with the majority being straight and averaging 105 nm in diameter. The straight nanowires varied in widths, but appeared highly uniform along the length individually (Fig. 3a-c, 4b). The straight nanowire is shown as stacked crystal layers with high crystallinity (Fig. 5b), manifested by the selected area electron diffraction (SAED) pattern shown in the inset. The beaded nanowires (Fig. 4c) appeared to be the self-assembly of elongated rods linked between enlarged heads and tapered tails, measured to be around 135 nm and 74 nm wide, respectively (Fig. 5c). Such a shape could be associated with epitaxial post-growths of straight rods.[32, 33] The bamboo-like nanowires showed wider joints (Fig. 5d) and were thought to be associated with high stacking faults.[9] Both the beaded and bamboo-like nanowires had more ragged surfaces (Fig. 4c,d). All these nanowires were found to separate from the nanoparticle-filled fibers. These distinctly different fiber size reduction and fibrous mat morphologies suggest different pyrolytic behaviors between the two composites.

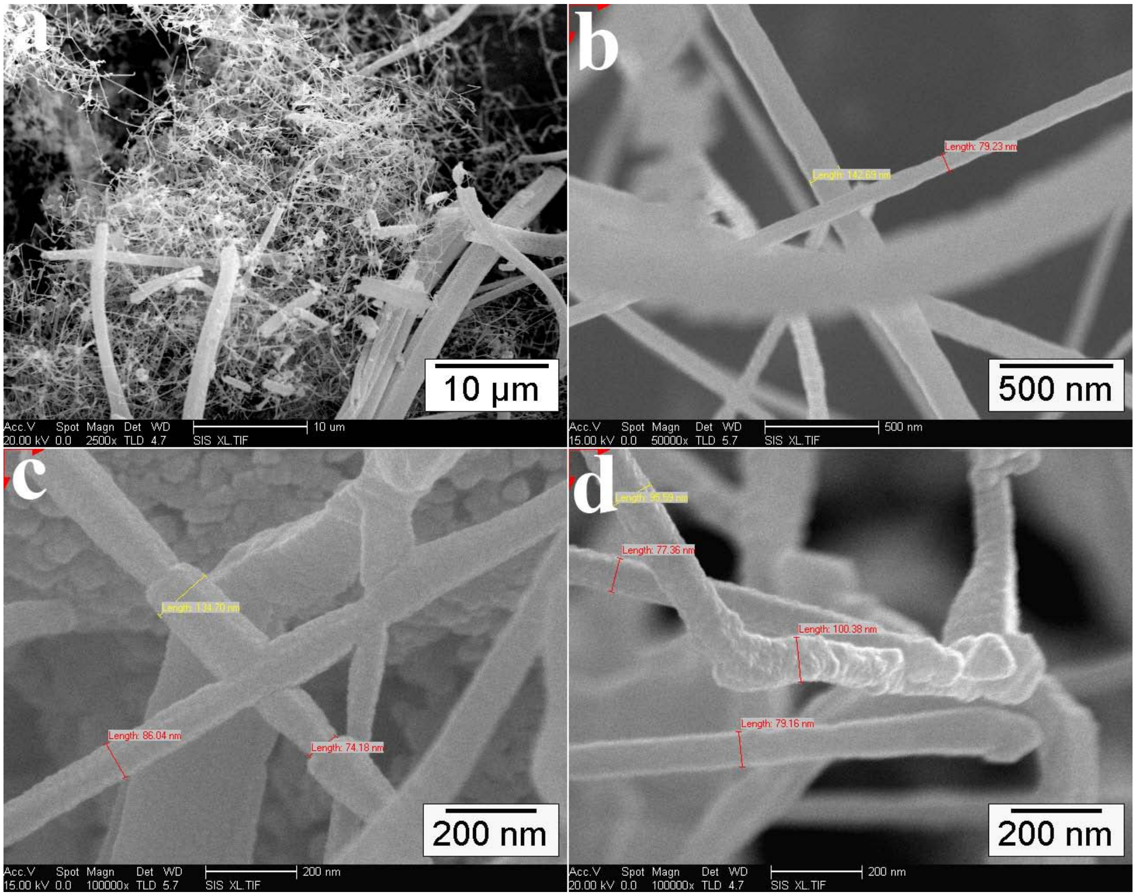

Fig. 4 SEMs of PUS/PMMA pyrolyzed at 1560ºC for 3 h in argon: (a) sheath-core fiber segments and high concentration of nanowires; nanowires with: (b) rod, (c) beaded, and (d) bamboo-like morphologies.

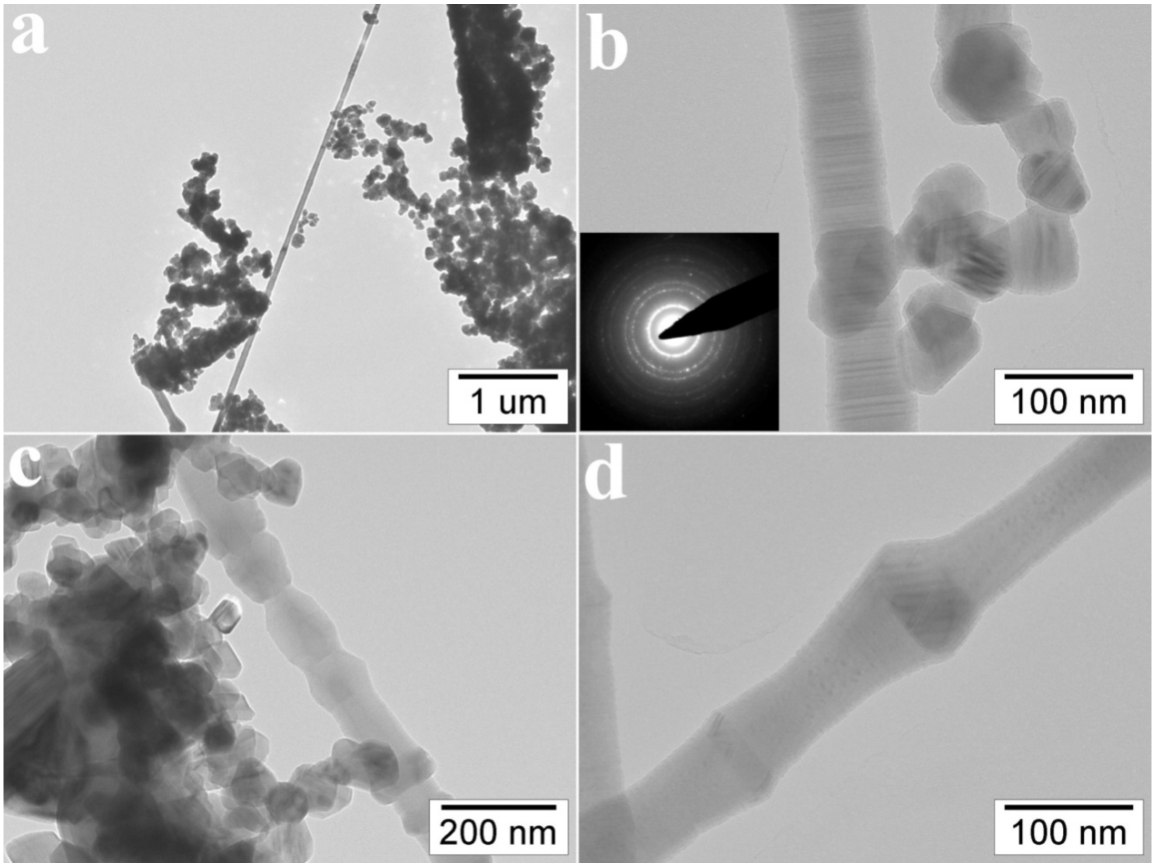

Fig. 5 TEMs of nanowires from pyrolyzing PUS/PMMA at 1560ºC in: (a, b) straight rod, (c) beaded, (d) bamboo-like shapes.

Thermal transformation and pyrolysis

Both PMMA and PS are known to decompose to leave little carbon residues at temperatures above 500ºC in either inert or oxygenated environment. This complete pyrolytic behavior along with the facile electrospinnability to form fibers is the main reason for their selection as the polymer matrices for PUS. Both PMMA and PS lost 100% mass upon heating to 460ºC (a and c in Fig. 6B), but the majority of mass loss of PMMA began at 265ºC, about 100ºC lower than PS. The different thermal decomposition pathways were more clearly shown in their DSC thermograms (Fig. 6A). PMMA lost 3.5%, 31.5%, and 63.2% mass in 180-265, 265-330, and 330-460ºC temperature ranges (a in Fig. 6B), respectively, with the latter two generally coinciding with the two DSC endotherms at 235-320 and 320-383ºC (Fig. 6A, curve a). The initial small mass loss of PMMA is commonly associated with the loss of residual monomers and the major mass loss is due to chain decomposition and scission to generate combustible gaseous molecules that burn in final step to form water, carbon dioxide and other small molecules.[34, 35] PS showed a gradual on-set of endotherm at around 250ºC and peaked at around 415ºC and a very sharp 100% mass loss in a narrow temperature range of 365-456ºC. This is consistent with the known pyrolytic decomposition of PS through unzipping chain scission or depolymerization to monomer and other aromatic hydrocarbons and their subsequent evaporation.[36, 37] The major difference in the thermal decomposition pathways between PMMA and PS is the combustion of the PMMA decomposition products at above 420ºC due to the presence of oxygen in its structure.[38, 39] This is confirmed by the PMMA exotherm centered at 418ºC that is absent in PS (Fig. 6A).

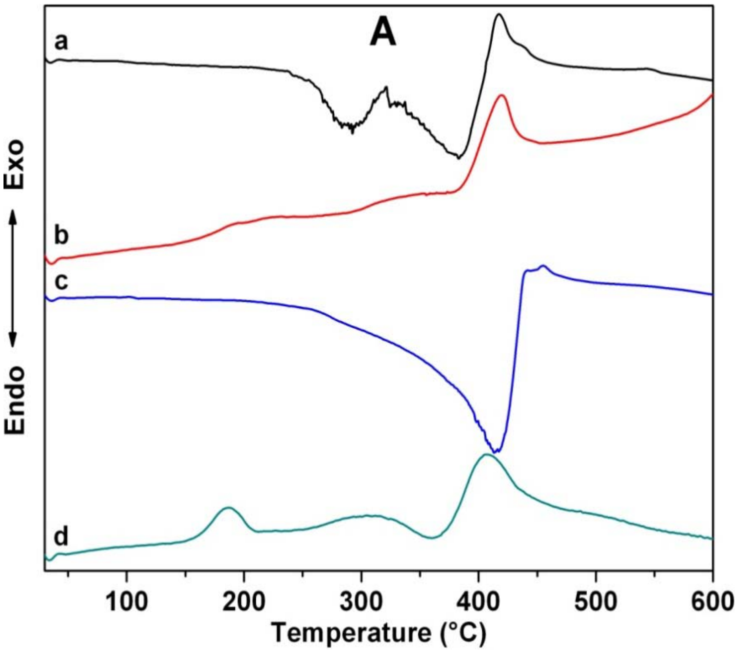

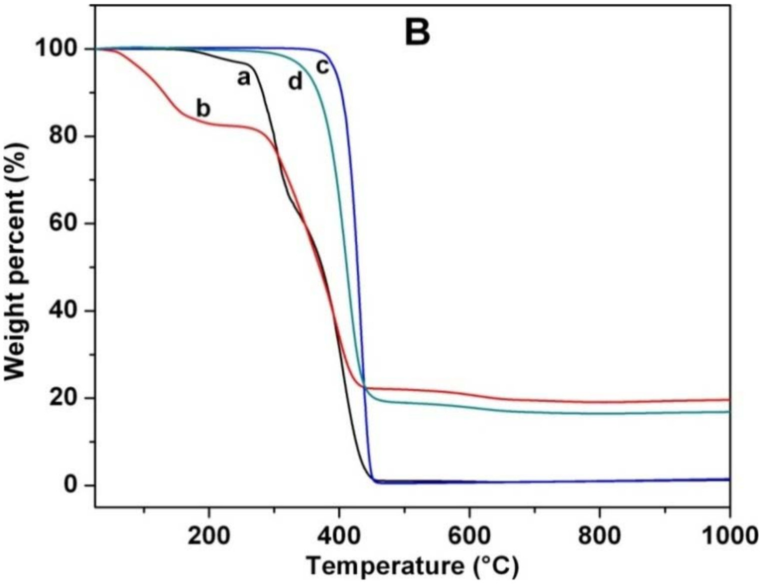

Fig. 6 (A) DSC and (B) TGA showing the thermal behaviors of (a) PMMA, (b) PUS/PMMA, (c) PS, (d) PUS/PS.

PUS is readily thermoset into solid upon heating close to 200ºC, then pyrolyzed into silicon carbide or silicon nitride up to 1000ºC. PUS exhibited two endotherms around 171 and 301ºC and three mass losses of about 22%, 5% and 7.4% at 300ºC, 500ºC and 750ºC, respectively, yielding 65% ceramic solid.[40] The major mass loss associated with crosslinking and decomposition of organic side groups of the preceramic PUS and evident by the endotherms up to 500ºC, the same temperature range in which PMMA and PS completely decompose. The few percent mass loss between 500ºC and 750ºC is associated with redistribution reactions and dehydrogenation.

The DSC of PUS/PMMA had little resemblance of that of PUS, but exhibited a clear exotherm at around 420ºC, same as PMMA (b in Fig. 6A). The TGA of PUS/PMMA, on the other hand, showed a 22% mass loss at 300ºC that was not only similar, but in fact, proportional to the PUS content in the composite (b in Fig. 6B). The final residue at 20% was not only higher than what is expected from the 25% PUS content in the PUS/PMMA composite but also was achieved at a slightly lower temperature of 700ºC. These thermal analyses of PUS/PMMA indicate that PUS in the composite did crosslink and decompose, but the molten PMMA (T_m~160ºC) may interfere with the chemical pathways in both crosslinking and decomposition of PUS.

The TGA of PUS/PS resembled that of PS, only at a lower onset temperature, showing 17% residue, also higher than what is expected from the 20% PUS in the PUS/PMMA composite (d in Fig. 6B). The DSC of PUS/PS showed a clear exotherm at 186ºC, evident of PUS crosslinking, and a new large exotherm at 406ºC, but no clear endotherm associated with PUS decomposition around 300ºC (d in Fig. 6A). These thermal analysis results suggest that the higher melting (T_m ~240ºC) PS did not interfere the crosslinking of PUS as PMMA, but may affect PUS decomposition, corroborated by the strong exotherm that followed.

Atomic compositions and chemical structures

The distinct thermal behaviors and decomposition pathways of PMMA and PS have shown great effects on the product morphologies and thermal crosslinking and structural transformation of PUS. The chemical compositions of the pyrolyzed PUS/PMMA and PUS/PS were further elucidated. The EDS mappings of Si, C and O on the SEM clearly showed the carbon signal in the pyrolyzed product at 1560ºC from PUS/PS was much stronger than that from PUS/PMMA (Fig. 7), corroborating the measured 75.3% and 52.1% C, respectively (Table 1). At either 1000ºC or 1560ºC, the pyrolyzed products from PUS/PS had consistently higher carbon and lower oxygen contents than those from PUS/PMMA. The pyrolyzed product from PUS/PMMA at 1000ºC had 32.5% O and nearly similar proportions of C and Si. This high O composition indicates that the infiltration of molten PMMA among the PUS molecules not only affects PUS crosslinking, but also possibly some or all of the subsequent reactions of PUS, i.e., decomposition, redistribution and dehydrogenation, at up to 1000ºC. The exothermic oxidation reaction between PUS and PS consumes most of the oxygen and leaves only 6.6% O but 74.7% C in the intermediate pyrolyzed product at 1000ºC. Pyrolysis at 1560ºC left little O in both composite precursors. It should be noted that the atomic compositions calculated from EDS are semi-quantitative, sufficient to illustrate their relative changes, but not absolute values.

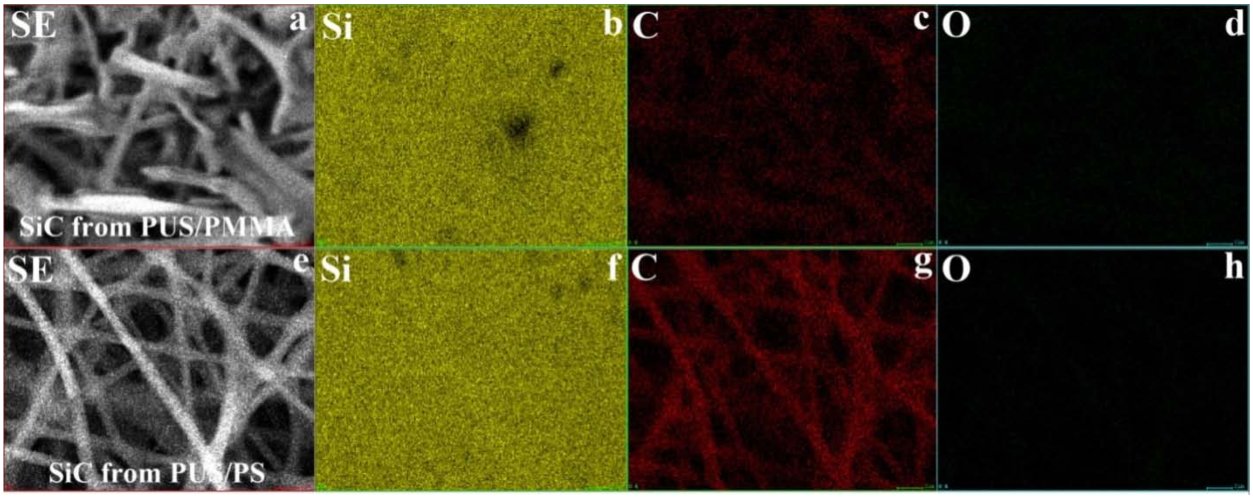

Fig. 7 EDS mappings of SiC from (a, b, c, d) PUS/PMMA and (e, f, g, h) PUS/PS pyrolyzed at 1560ºC for 3 h in argon. (grey: SEM; yellow: Si; red: C; green: O; black: background)

Table 1. Atomic compositions (atom%) of pyrolyzed products of PUS/PMMA and PUS/PS by EDS

Element	PUS/PMMA		PUS/PS	
	1000ºC	1560ºC	1000ºC	1560ºC
Si	30.9	43.9	18.7	22. 9
C	36.6	52.1	74.7	75.3
O	32.5	4.0	6.6	1.8

In PUS-derived SiCO, overall carbothermal reduction of SiO_2 by C to SiC can be written as (1):[41, 42]

$SiO_2(s) + 3C(s) \rightarrow SiC(s) + 2CO(g)$ (1)

It is generally accepted that SiC forms through the intermediate gaseous SiO. Thus, the above overall carbothermal reduction can be broken into two fundamental steps (2-3):[43]

$SiO_2(s) + C(s) \rightarrow SiO(g) + CO(g)$ (2)

$SiO(g) + 2C(s) \rightarrow SiC(s) + CO (g)$ (3)

Furthermore, the growth of SiC nanowires is believed to involve a gas-gas reaction illustrated as (4):[32, 44]

$SiO(g) + 3CO(g) \rightarrow SiC(s) + 2CO_2(g)$ (4)

Considering the gas-solid reaction nature of the carbothermal reduction shown in step (3), a high partial pressure of gaseous SiO generated by step (2) as well as the constant removal of CO from the reaction environment is required to drive the overall reaction (1) to proceed favorably toward SiC formation.

Due to the higher O content in the pyrolyzed PUS-PMMA, SiO_2 (Si-O bonded parts) is thought to be in higher proportion in the nanoporous SiCO sheath-core fibers. Gasification of SiO_2 to SiO, accompanied by the reactions with solid phase C, may cause the SiCO structure to be unstable, leading to the collapse of the 3D fibrous mat and the individual fibers as seen in Fig. 1c and Fig. 3a. Furthermore, the high porosity as well as the lack of immediate carbon source may quicken the diffusion and release of gaseous SiO from the fibers, generating the SiC nanowires outside the original fibers as seen in Fig. 3a-c. On the contrary, the structural stability of nanoporous SiCO sheath-core fibers derived from PUS/PS is much enhanced by the low SiO_2 and high C contents, in which the majority of the fiber mass remains in solid form during carbothermal reduction at 1560ºC, preserving the nanoporous sheath-core morphology in the final products (Fig. 3d-f). Moreover, the resultant intermediate gaseous SiO is very likely trapped inside the fibers and reacted readily with the abundant C in the surrounding area, preventing the formation of SiC nanowires out of the fibers. After carbothermal reduction, SiCO from both PUS/PMMA and PUS/PS were successfully converted to SiC with a trace amount of O, as shown by EDS mapping (Fig. 7 and Table 1).

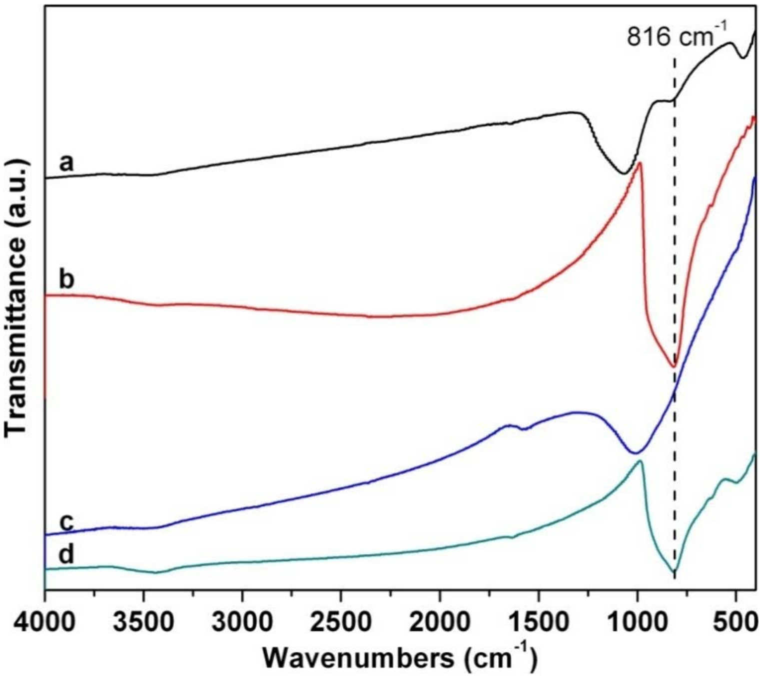

Fig. 8 FTIR spectra of PUS/PMMA pyrolyzed at (a) 1000ºC (b) 1560ºC and PUS/PS pyrolyzed at (c) 1000ºC (d) 1560ºC for 3 h in argon.

The structural evolution from SiCO to SiC was further elucidated by FTIR (Fig. 8). The SiCO derived from PUS/PMMA at 1000ºC showed two broad peaks centered at 1065 and 460 cm^{-1}, characteristic of Si-O-Si stretching.[45] The 816 cm^{-1} peak, corresponding to the Si-C vibration (curve a), intensified and widened significantly (curve b) upon pyrolysis at 1560ºC, indicating the formation of cubic SiC (β-SiC),[44] at the expense of the Si-O bands. SiCO derived from PUS/PS (curve c) showed a broad peak at 1005 cm^{-1} that is very likely the overlapping absorptions of low quantity of Si-O (1065 cm^{-1}) with the more abundant Si-C (816 cm^{-1}) present in the structure. The 1005 cm^{-1} peak of SiCO derived from PUS/PS at 1560ºC is also shifted to 816 cm^{-1} (curve d), suggesting the successful transformation of SiCO to β-SiC.[46]

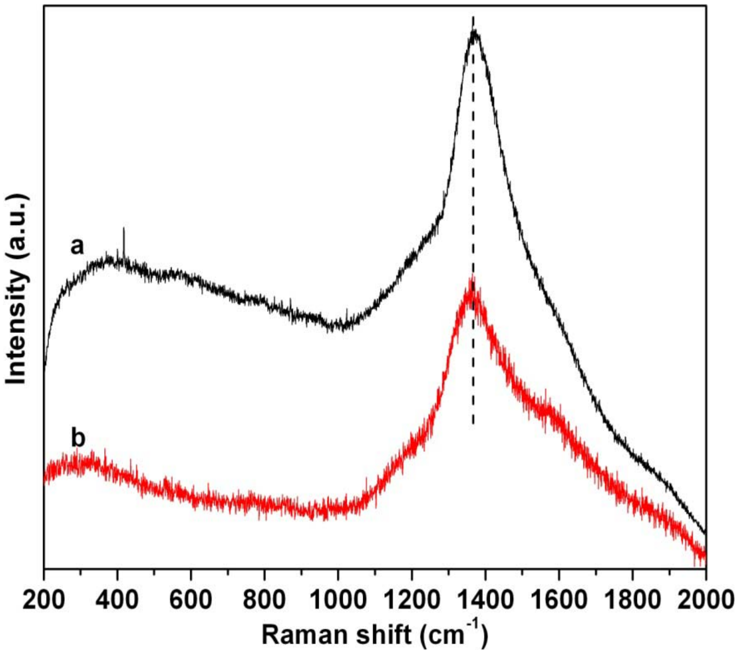

Fig. 9 Raman spectra of SiC pyrolyzed (1560ºC for 3 h in argon) from: (a) PUS/PMMA and (b) PUS/PS.

Raman spectra of SiC fibers from pyrolyzing PUS/PMMA and PUS/PS at 1560ºC show strong peaks at 1370 cm^{-1} (D band) characteristic of sp^3 bonding of carbon-containing materials.[47] The stronger shoulder peak at 1600 cm^{-1} (G band) in the spectra of SiC from PUS/PS corresponds to the sp^2 bonding in ordered graphite nanodomain,[26] agreed well with the higher 75.3% C content (Table 1) and the stronger C signals in EDS mapping (Fig. 7g). In comparison, the G band of SiC derived from PUS/PMMA is almost invisible, consistent with the nearly 1/1 Si/C atomic ratio in the final SiC structure and weak carbon signal shown in Fig. 7c.

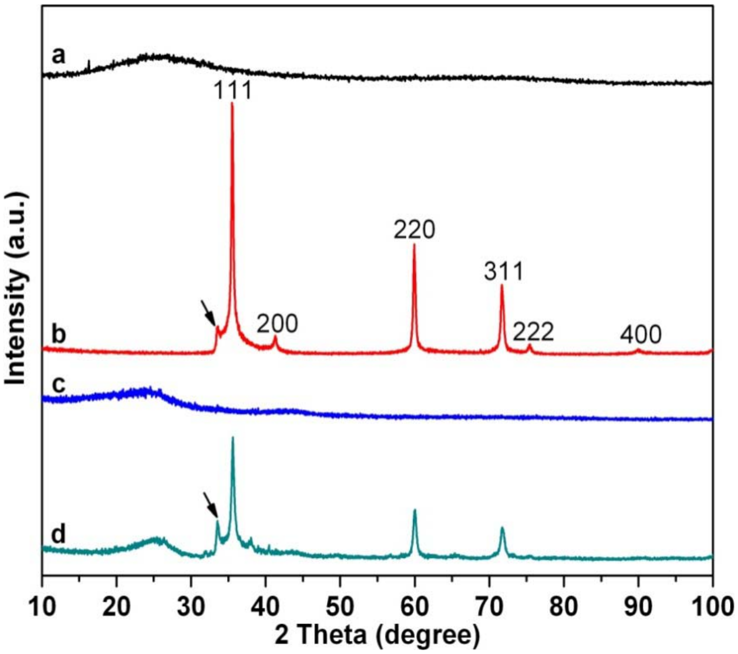

Fig. 10 XRD patterns of SiC (SiCO) from (a, b) PUS/PMMA and (c, d) PUS/PS pyrolyzed at (a, c) 1000ºC and (b, d) 1560ºC. The indexed peaks in (b, d) correspond to the β-SiC structure and the peaks marked by arrows are caused by stacking faults or a trace amount of α-SiC.

The successful structural conversions from amorphous SiCO to polycrystalline cubic SiC were further confirmed by XRD (Fig. 10). Both pyrolysis products from PUS/PMMA and PUS/PS at 1000ºC showed only a broad peak centered around 2θ = 24º (curves a and c), typical of amorphous silica[48] and carbon.[25] These amorphous silica and carbon peaks disappeared in the spectra of both pyrolysis products at 1560ºC. The presence of three strong peaks at 2θ = 35.7, 60.0, and 71.8º, corresponding to 111, 220, 311 lattice planes of β-SiC,[26] respectively, confirms the successful synthesis of face-centered cubic SiC or β-SiC from carbothermal reduction. This is in agreement with the standard JCPDS card (No.74-2307). Relatively weak peaks at 2θ = 41.4, 75.5, and 90.0º, assigned to 200, 222, and 400 planes,[5] are also found in the spectra of SiC derived from PUS/PMMA but not visible in that of PUS/PS, indicating the higher purity of β-SiC in the former. The marked weak peak at 2θ = 33.6º could be due to the stacking faults or the trace amount of α-SiC.[13] In addition to β-SiC, graphite peak at 2θ = 26.4º (002)[49] was also observed for SiC from PUS/PS but not that from PUS/PMMA, which is in accordance with the results from EDS and Raman. Furthermore, weak diffraction peaks close to 2θ = 40º as well as the enhanced peak at 2θ = 33.6 (curve d) also suggest trace amounts of the hexagonal α-SiC attributed to the stacking faults along the growth axis in the PUS/PS derived fibers.[9]

Conclusions

Nanoporous SiC fibers with varied compositions and morphologies were successfully fabricated by electrospinning preceramic PUS mixed with either PMMA or PS and converting to ceramics by pyrolysis in argon at 1560ºC. The distinct thermal behaviors and decomposition pathways of PMMA and PS influenced the morphologies, chemical compositions and crystal forms of SiC fibers. Pyrolysis of PUS/PMMA and PUS/PS at 1000ºC generally led to fibrous mats of amorphous SiCO or silica and carbon with 32.5% and 6.6% O, respectively, and the latter with high C content (74.7%). Pyrolysis at 1560ºC effectively minimized the O content and produced in polycrystalline cubic SiC (β-SiC) structures in the ceramic fibers from both composites. The SiC fibers pyrolyzed from PUS/PMMA contained higher purity β-SiC and are in an interconnected fibrous mat of nanoparticle-filled porous core and wrinkled sheath whereas those from PUS/PS were fragmented nanoparticle-filled porous fibers intermixed with abundant 100 nm diameter nanowires with straight, beaded, and bamboo-like morphologies that also showed the presence of graphite and α-SiC. The nanoporous SiC sheath-core fibers could be an excellent supporting material for the heterogeneous catalysis due to its thermal and chemical stability as well as high porosity. The resultant SiC nanowires could also find broad applications as drug carriers, semiconductive materials for electronics, reinforcing fillers for high strength ceramics, etc.

Acknowledgements

This research was made possible by funding from the U.S. National Science Foundation (grant CMMI #0700272) and National Textile Center (project M02-CD05) as well as the Jastro-Shields Graduate Research Award and Summer Graduate Researcher Award from the University of California, Davis.

References

1. C. R. Eddy, Jr. and D. K. Gaskill, *Science*, 2009, **324**, 1398-1400.
2. K. Bourenane, A. Keffous, G. Nezzal, A. Bourenane, Y. Boukennous and A. Boukezzata, *Sens. Actuators, B*, 2008, **B129**, 612-620.
3. S. E. Saddow, A. Agarwal and ebrary Inc, Artech House, Boston, 2004, pp. xiii, 212 p.
4. W. Lien, N. Ferralis, C. Carraro and R. Maboudian, *Cryst. Growth Des.*, **10**, 36-39.
5. L. Gu, D. Ma, S. Yao, X. Liu, X. Han, W. Shen and X. Bao, *Chem.--Eur. J.*, 2009, **15**, 13449-13455.
6. P. Krawiec, C. Schrage, E. Kockrick and S. Kaskel, *Chem. Mater.*, 2008, **20**, 5421-5433.
7. I.-K. Sung, M. Mitchell, D.-P. Kim and P. J. A. Kenis, *Adv. Funct. Mater.*, 2005, **15**, 1336-1342.
8. R. M. Feenstra and C. E. C. Wood, *Porous silicon carbide and gallium nitride : epitaxy, catalysis, and biotechnology applications*, John Wiley & Sons, Chichester, England ; Hoboken, NJ, 2008.
9. E. Vanhaecke, S. Ivanova, A. Deneuve, O. Ersen, D. Edouard, G. Wine, P. Nguyen, C. Pham and C. Pham-Huu, *J. Mater. Chem.*, 2008, **18**, 4654-4662.
10. Z. Zhang, F. Wang, X. Yu, Y. Wang and Y. Yan, *J. Am. Ceram. Soc.*, 2008, **92**, 260-263.
11. I. Florea, M. Houlle, O. Ersen, L. Roiban, A. Deneuve, I. Janowska, P. Nguyen, C. Pham and C. Pham-Huu, *J. Phys. Chem. C*, 2009, **113**, 17711-17719.
12. Y.-H. Park, T. Hinoki and A. Kohyama, *J. Nucl. Mater.*, 2009, **386-388**, 1014-1017.
13. B.-H. Yoon, C.-S. Park, H.-E. Kim and Y.-H. Koh, *J. Am. Ceram. Soc.*, 2007, **90**, 3759-3766.
14. K. Wang, H. Wang and Y.-B. Cheng, *Chem. Commun. (Cambridge, U. K.)*, **46**, 303-305.
15. Y.-J. Jin and Y.-W. Kim, *J. Mater. Sci.*, **45**, 282-285.
16. W.-C. Lien, N. Ferralis, A. P. Pisano, C. Carraro and R. Maboudian, *Appl. Phys. Lett.*, 2009, **95**, 101901/101901-101901/101903.
17. S.-H. Chae, Y.-W. Kim, I.-H. Song, H.-D. Kim and M. Narisawa, *J. Eur. Ceram. Soc.*, 2009, **29**, 2867-2872.
18. M. Fukushima, Y. Zhou and Y.-i. Yoshizawa, *J. Membr. Sci.*, 2009, **339**, 78-84.
19. J.-H. Eom and Y.-W. Kim, *J. Mater. Sci.*, 2009, **44**, 4482-4486.
20. S. Shimada, M. Murata and M. Narisawa, *J. Am. Ceram. Soc.*, 2008, **92**, 21-25.

21. S. Liu, Y.-P. Zeng and D. Jiang, *Ceram. Int.*, 2009, **35**, 597-602.
22. Y.-W. Kim, J.-H. Eom, C. Wang and C. B. Park, *J. Am. Ceram. Soc.*, 2008, **91**, 1361-1364.
23. S. Shiraishi, A. Kikuchi, M. Sugimoto and M. Yoshikawa, *Chem. Lett.*, 2008, **37**, 574-575.
24. A. R. Maddocks and A. T. Harris, *Mater. Lett.*, 2009, **63**, 748-750.
25. G. Hasegawa, K. Kanamori, K. Nakanishi and T. Hanada, *J. Mater. Chem.*, 2009, **19**, 7716-7720.
26. Y. Cheng, J. Zhang, Y. Zhang, X. Chen, Y. Wang, H. Ma and X. Cao, *Eur. J. Inorg. Chem.*, 2009, 4248-4254.
27. S. Sarkar, A. Chunder, W. Fei, L. An and L. Zhai, *J. Am. Ceram. Soc.*, 2008, **91**, 2751-2755.
28. B. M. Eick and J. P. Youngblood, *J. Mater. Sci.*, 2009, **44**, 160-165.
29. H. A. Liu and K. J. Balkus, *Mater. Lett.*, 2009, **63**, 2361-2364.
30. J. Li, Y. Zhang, X. Zhong, K. Yang, J. Meng and X. Cao, *Nanotechnology*, 2007, **18**, 245606/245601-245606/245604.
31. P. Lu, Q. Huang, B. Liu, Y. Bando, Y.-L. Hsieh and A. K. Mukherjee, *J. Am. Chem. Soc.*, 2009, **131**, 10346-10347.
32. J. Wei, K. Z. Li, H. J. Li, Q. G. Fu and L. Zhang, *Mater. Chem. Phys.*, 2006, **95**, 140-144.
33. Y. J. Hao, J. B. Wagner, D. S. Su, G. Q. Jin and X. Y. Guo, *Nanotechnology*, 2006, **17**, 2870-2874.
34. W. R. Zeng, S. F. Li and W. K. Chow, *J. Fire Sci.*, 2002, **20**, 401-433.
35. J. D. Peterson, S. Vyazovkin and C. A. Wight, *J. Phys. Chem. B*, 1999, **103**, 8087-8092.
36. A. I. Roland and G. Schmidt-Naake, *J. Anal. Appl. Pyrolysis*, 2001, **58-59**, 143-154.
37. B. N. Jang and C. A. Wilkie, *Polymer*, 2005, **46**, 2933-2942.
38. M. C. Costache, D. Wang, M. J. Heidecker, E. Manias and C. A. Wilkie, *Polym. Adv. Technol.*, 2006, **17**, 272-280.
39. S. Bourbigot, J. W. Gilman and C. A. Wilkie, *Polym. Degrad. Stab.*, 2004, **84**, 483-492.
40. P. Lu, Q. Huang, A. Mukherjee and Y.-L. Hsieh, *J. Phys. Chem. C*, 2010, **114**, 11776-11782.

41. A. Bachmatiuk, F. Borrnert, M. Grobosch, F. Schaffel, U. Wolff, A. Scott, M. Zaka, J. H. Warner, R. Klingeler, M. Knupfer, B. Buchner and M. H. Rummeli, *Acs Nano*, 2009, **3**, 4098-4104.

42. S. Galvagno, S. Portofino, G. Casciaro, S. Casu, L. d'Aquino, M. Martino, A. Russo and G. Bezzi, *J. Mater. Sci.*, 2007, **42**, 6878-6886.

43. J.-S. Lee, S.-H. Lee and S.-C. Choi, *J. Alloys Compd.*, 2009, **467**, 543-549.

44. L. F. Chen, Z. H. Cai, L. Zhang, L. Lan, X. J. Chen and J. Zeng, *J. Mater. Sci.*, 2007, **42**, 1004-1009.

45. Y. Ding and H. Shirai, *J. Appl. Phys.*, 2009, **105**, 043515/043511-043515/043514.

46. S. Gallis, V. Nikas, M. Huang, E. Eisenbraun and A. E. Kaloyeros, *J. Appl. Phys.*, 2007, **102**, 024302/024301-024302/024309.

47. A. Tamayo, J. Rubio, R. Pena-Alonso, F. Rubio and J. L. Oteo, *J. Eur. Ceram. Soc.*, 2008, **28**, 1871-1879.

48. J. Latournerie, P. Dempsey, D. Hourlier-Bahloul and J. P. Bonnet, *J. Am. Ceram. Soc.*, 2006, **89**, 1485-1491.

49. Z. J. Zhang, F. C. Wang, X. D. Yu, Y. W. Wang, Y. H. Yan, K. Li and Z. Q. Luan, *J. Am. Ceram. Soc.*, 2009, **92**, 260-263.